

# 3D-TRANSFORMER: MOLECULAR REPRESENTATION WITH TRANSFORMER IN 3D SPACE

Fang Wu<sup>1,2</sup>, Qiang Zhang<sup>2\*</sup>, Dragomir Radev<sup>4</sup>, Jiyu Cui<sup>3</sup>, Wen Zhang<sup>2</sup>, Huabin Xing<sup>3</sup>, Ningyu Zhang<sup>2</sup>, Huajun Chen<sup>2</sup>\*

<sup>1</sup> Columbia University

<sup>2</sup> Department of Computer Science and Technology, Zhejiang University

<sup>3</sup> Department of Chemical and Biochemical, Zhejiang University

<sup>4</sup> Department of Computer Science, Yale University

fw2359@columbia.edu

{qiang.zhang.cs, wenzhang2015, xinghb, huajunsir}@zju.edu.cn

dragomir.ralev@yale.edu

## ABSTRACT

Spatial structures in the 3D space are important to determine molecular properties. Recent papers use geometric deep learning to represent molecules and predict properties. These papers, however, are computationally expensive in capturing long-range dependencies of input atoms; and more importantly, they have not considered the non-uniformity of interatomic distances, thus failing to learn context-dependent representations at different scales. To deal with such issues, we introduce Molformer, a variant of the Transformer for molecular representations that incorporates 3D spatial information. Molformer operates on a fully-connected graph with direct connections between atoms. To cope with the non-uniformity of interatomic distances, we develop a multi-scale self-attention module that exploits local fine-grained patterns with increasing contextual scales. As molecules of different sizes rely on different kinds of spatial features, we design an adaptive position encoding module that adopts different position encoding methods for small and large molecules. Finally, to attain the molecular representation from atom embeddings, we propose an attentive farthest point sampling algorithm that selects a portion of atoms with the assistance of attention scores, overcoming handicaps of the virtual node and previous distance-dominant downsampling methods. We validate Molformer across three important scientific domains: quantum chemistry, material science, and proteomics. Our experiments show significant improvements over state-of-the-art models on the crystal property prediction task and the protein-ligand binding affinity prediction task, and show better or competitive performance in quantum chemistry molecular datasets. This work provides clear evidence that biochemical tasks can gain consistent benefits from 3D molecular representations and different tasks require different position encoding methods.

## 1 INTRODUCTION

Spatial structures are among the most crucial factors to decide molecular properties and understand their principles of action in the physical world. For example, 3D spatial structures of proteins provide valuable information for inferring biological interventions, such as structure-based drug development and targeted mutagenesis (Senior et al., 2020; Jumper et al., 2021; Baek et al., 2021). In chemistry, zeolites show obvious differences in catalytic and separation properties caused by subtle changes in the 3D structure, which could not be detected from their chemistry compositions (Chai et al., 2020; Pfriem et al., 2021). Apart from that, in the pharmaceutical industry, the same compounds can have completely different 3D structures due to different crystal shapes, and thus can have significantly different solubility, melting point, dissolution and bioavailability (Zhang et al., 2017). To sum up, capturing 3D spatial structures is essential to accurately forecast molecular properties.

\*Coresponding author.

Based on these facts, researchers have studied molecular representation learning techniques (Rao et al., 2019) to include 3D spatial information (Zhavoronkov et al., 2019).

The dominant 3D molecular learning models are Graph Neural Networks (GNNs) and 3D Convolutional Neural Networks (3DCNNs) (Derevyanko et al., 2018; Pagès et al., 2019; Townshend et al., 2019). GNNs create edges by using either chemical bonds or finding the neighbors of each node within a distance cutoff (Zhang et al., 2020). They encode pairwise connectivity of atoms in a non-Euclidean space and require running multiple hops for an atom to reach to another. 3DCNNs are able to deal with translational and permutational symmetries, but need to stack as many layers as possible to build direct connections between remote regions, incurring significant computational costs. In contrast, Transformers rely on the self-attention mechanism to capture long-term dependencies (Hernández & Amigó, 2021) in parallel. This allows atoms to interact with each other regardless of their input order or pairwise distances in 3D space. Meanwhile, Equivariant Neural Networks (ENNs) (Thomas et al., 2018) have emerged as a new class of methods, where geometric transformations of their inputs lead to well-defined transformations of outputs. Some ENNs (Fuchs et al., 2020) adopt Transformers as the backbone. However, the Transformer architecture has several intrinsic drawbacks, including its insensitivity to local patterns among non-uniformly distancing atoms and its inefficiency to aggregate atom features. These ENNs fail to surmount these drawbacks.

In this work, we present the Molformer on the basis of all preceding analysis. It takes the raw 3D coordinates and atom types as the input. The Transformer operates on a fully-connected graph with direct connections between atoms at remote positions (Veličković et al., 2017; Joshi, 2020), which reduces computational burden of multi-hop GNNs and stacked 3DCNNs. However, this characteristic limits Transformer’s capacity in exploiting local structures and leads to poor generalization in unseen cases (Qi et al., 2017b). Therefore, the proposed Molformer model contains a Multi-scale Self-Attention (MSA) module to recognize fine-grained patterns from neighborhoods. Moreover, we introduce an AdapTive Position Encoding (ATPE) module, which adaptively selects different types of position encoding methods for different molecules. For small molecules<sup>1</sup> with graph-like structures, ATPE utilizes a roto-translation invariant Convolutional Position Encoding (CPE) to depict position relationship among atoms and their adjacencies. For larger structures such as proteins and crystal materials, which we collectively call large molecules, ATPE employs an Absolute Position Encoding (APE) for better representations of their 3D conformations. After that, to retain a comprehensive representation of the entire molecule, we propose an Attentive Farthest Point Sampling (AFPS) module that selects important atoms with the assistance of the attention score map. To summarize, our contributions are as follows:

- To the best of our knowledge, Molformer is the first Transformer variant that incorporates 3D spatial information for molecular representation learning.
- The proposed MSA is a novel self-attention implementation with continually incremental contextual scales to extract local patterns from non-uniformly distancing atoms.
- The ATPE method adopts different position encoding strategies according to a newly designed metric for structural complexity measurement. For small and simple molecules, we develop a roto-translation invariant CPE method in ATPE to encode relative distance of each atom and their neighbors at a linear computational time cost, and use an APE method to portray 3D conformations of large and complex molecules.
- To obtain the molecular representation based on atom features, we design a simple yet effective downsampling algorithm named AFPS that considers both the spatial distances and the importance of each atom.
- We conduct extensive experiments in domains of quantum chemistry, materials science, and proteomics, and show significant improvements on several benchmarks. We also show that Molformer is robust to multiple molecular conformations. Code and all datasets are available at <https://github.com/smiles724/Molformer>.

<sup>1</sup>[https://en.wikipedia.org/wiki/Small\\_molecule](https://en.wikipedia.org/wiki/Small_molecule)

## 2 PROBLEM DEFINITION AND PRELIMINARIES

### 2.1 PROBLEM DEFINITION

A molecule  $\mathcal{S} = (\mathbf{E}, \mathbf{P})$  has  $N$  atoms and  $C$  atom classes, where  $\mathbf{E} = \{e_1, \dots, e_N\} \in \mathbb{R}^{N \times C}$  contains the one-hot atom representations and  $\mathbf{P} = \{p_1, \dots, p_N\} \in \mathbb{R}^{N \times 3}$  contains the 3D coordinates of each atom. Each one-hot  $e_i$  can be converted to a dense vector  $\mathbf{x}_i = e_i \mathbf{W}^E$ , with  $\mathbf{x}_i \in \mathbb{R}^{d_{model}}$  and  $\mathbf{W}^E \in \mathbb{R}^{C \times d_{model}}$  being the embedding matrix. The 3D coordinates of the atom  $i$  is a three-dimensional vector  $\mathbf{p}_i = [p_i^x, p_i^y, p_i^z]$ .

A representation learning model  $f$  acts on  $\mathcal{S}$ , obtaining its representation  $\mathbf{r} = f(\mathcal{S})$ . For unpaired downstream tasks such as chemical property prediction,  $\mathbf{r}$  is forwarded to a prediction model  $g$  and attain the prediction  $\hat{y} = g(\mathbf{r})$ . For paired tasks like ligand binding affinity prediction, the prediction model  $g$  takes as input the two molecules and outputs their relationship  $\hat{y} = g(\mathbf{r}_1, \mathbf{r}_2)$ .

### 2.2 PRELIMINARIES

**Self-attention Mechanism.** The Transformer (Vaswani et al., 2017) has become very successful due to its core component, self-attention. Given a set of input features  $\{\mathbf{x}_i\}_{i=1, \dots, N}$ , the standard dot-product attention layer is as the following:

$$\mathbf{q}_i = f_Q(\mathbf{x}_i), \mathbf{k}_i = f_K(\mathbf{x}_i), \mathbf{v}_i = f_V(\mathbf{x}_i), a_{ij} = \mathbf{q}_i \mathbf{k}_j^T / \sqrt{d_k}, \mathbf{z}_i = \sum_{j=1}^N \sigma(a_{ij}) \mathbf{v}_j \quad (1)$$

where  $\{f_Q, f_K, f_V\}$  are embedding transformations, and  $\{\mathbf{q}_i, \mathbf{k}_i, \mathbf{v}_i\}$  are respectively the query, key, and value vectors with the same dimension  $d_k$ .  $a_{ij}$  is the attention that the token  $i$  pays to the token  $j$ .  $\sigma$  denotes the *Softmax* function and  $\mathbf{z}_i$  is the output embedding of the token  $i$ . This formula conforms to a non-local network (Wang et al., 2018), indicating its inability to capture fine-grained patterns in a local context.

**Position Encoding.** Self-attention is invariant to permutation of the input (Dufter et al., 2021), and position encoding ensures that the Transformer will reveal positional information. Position encoding methods can be either based on absolute positions or relative distances. The former takes the raw position information as input and is sensitive to spatial transformations. The latter manipulates the attention score by incorporating relative distances (Guo et al., 2020a; Pan et al., 2021):  $a_{ij} = \mathbf{q}_i \mathbf{k}_j^T / \sqrt{d_k} + f_{PE}(\mathbf{p}_i - \mathbf{p}_j)$ , where  $f_{PE}(\cdot)$  is the position encoding function and is translation invariant. The rotation invariance can be further accomplished by taking a L2-norm  $\|\mathbf{p}_i - \mathbf{p}_j\|_2$  (Chen et al., 2019b). However, compressing a 3D molecule to a 2D graph using L2-norm will lose important spatial and geometric information.

## 3 MOLFORMER

To customize the Transformer architecture for molecular representation with 3D spatial information, we develop three major improvements: an adaptive position encoding module, a multi-scale self-attention module, and an attentive farthest point sampling module (see Figure 1).

### 3.1 ADAPTIVE POSITION ENCODING

Proper encoding of position information is important in the Transformer architecture. As different types of molecules have different 3D structure complexities, we design a simple but efficient metric to measure this molecular structure complexity in the 3D space. First, we need to find the smallest cuboid to cover the molecule with a length, height, wide of  $l, h, w$ . Then the metric is defined as:

$$\phi := \left( \frac{a}{b} + \frac{b}{c} - 1 \right) \tanh \left( \frac{N}{100} \right), \quad (2)$$

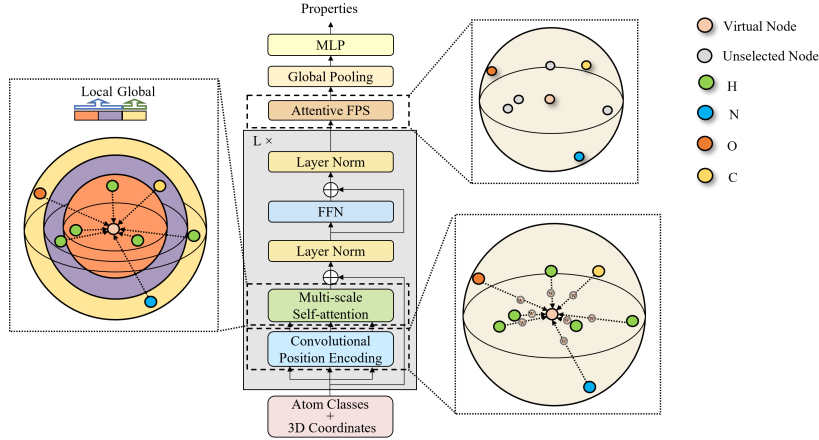


Figure 1: The overall architecture of our Molformer for small molecules. Local features are shown in purple and orange; yellow corresponds to a global feature.

where  $a = \min(l, h, w)$ ,  $c = \max(l, h, w)$  and  $b$  is the second largest of  $(l, h, w)$ . An intuitive explanation of such a metric is available at Appendix A.1. It can be easily shown that when  $a \approx b \ll c$  or  $a \ll b \approx c$ , the structure complexity is lower than the case of  $a \approx b \approx c$  where the molecule has a complex 3D structure, as shown in Figure 2.

Moreover, Townshend et al. (2020) show that small molecules are more efficiently represented as graph-like structures and their properties depend more on the relative distance of each atom to its adjacencies. While for larger molecules and complex 3D geometries, the exact positions of atoms and the overall conformations of the molecule play a more critical role in tasks like ligand-protein affinity prediction and crystal property prediction (Townshend et al., 2020). Based upon these analysis, we develop an adaptive position encoding method: atom position encodings are adaptively determined by molecular sizes and their 3D structure complexities as follows,

$$\text{ATPE} = \begin{cases} \text{CPE} & \phi < \tilde{\phi} \\ \text{APE} & \phi \geq \tilde{\phi} \end{cases} \quad (3)$$

where  $\tilde{\phi}$  is the threshold to separate small and large molecules. For small molecules with  $\phi < \tilde{\phi}$ , to enable rotation invariance and keep geometric information, instead of adding a term of  $f_{\text{PE}}(\mathbf{p}_i - \mathbf{p}_j)$ , we propose a CPE that applies a convolutional operation to the interatomic distance  $\mathbf{D} \in \mathbb{R}^{N \times N}$ :

$$\mathbf{A}_{\text{cov}} = \text{Conv}_{2d}(\mathbf{D}) \odot \mathbf{A}, \quad (4)$$

where  $\mathbf{A} = [a_{i,j}]_{i,j=1,\dots,N} \in \mathbb{R}^{N \times N}$  is the attention matrix,  $\text{Conv}_{2d}(\cdot)$  denotes a 2D shallow convolutional network with a kernel size of  $1 \times 1$ , and  $\odot$  is the element-wise product. With multi-headed self-attention,  $\mathbf{A}_{\text{cov}}$  is expanded in the sense that  $\mathbf{A}_{\text{cov}} \in \mathbb{R}^{H \times N \times N}$ , and  $\text{Conv}_{2d}(\cdot)$  has  $H$  output channels. The CPE method induces  $O(N)$  convolution operations on each atom and can drastically reduce training time when the number of atoms is very large (Wu et al., 2021). In what follows, we ignore the subscript cov from  $\mathbf{A}_{\text{cov}}$  to make it consistent with that of large molecules.

As for large molecules with thousands of covalently bonded atoms, relative distances are not able to capture geometric information of 3D spatial structures. We employ the absolute position information. In terms of the implementation of APE, we use the sinusoidal function-based absolute position encoding method (Li et al., 2019) to represent the 3D molecular conformations. More details are in Appendix A.2. We also analyse in Appendix A.3 that absolute positions are able to efficiently capture spatial information of chiral molecules that GNNs and ENNs are unable to differentiate.

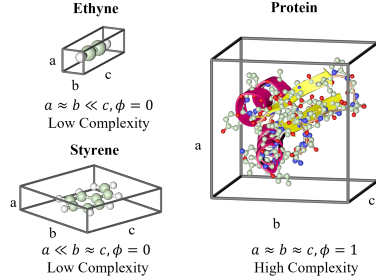


Figure 2: Molecular cuboids with different structure complexities. Ethyne and styrene are small molecules, while protein is a kind of large molecule.

---

**Algorithm 1** Pseudocode of Attentive Farthest Point Sampling

---

**Input:** The attention score matrix  $\mathbf{A} \in \mathbb{R}^{N \times N}$ , a Euclidean distance matrix  $\mathbf{D} \in \mathbb{R}^{N \times N}$ .**Output:**  $K$  sampled points.

- 1:  $\tilde{\mathbf{A}} \leftarrow \mathbf{A} \in \mathbb{R}^N$ ,  $\tilde{\mathbf{D}} \leftarrow \mathbf{D} \in \mathbb{R}^{N \times N}$
- 2:  $\mathcal{P} = \{x_{\#}\}$ ,  $\mathcal{M} = \{1, 2, \dots, N\}$
- 3: **while**  $\text{length}(\mathcal{P}) < k$  **do**
- 4:      $x_{\text{new}} = \underset{i \in \mathcal{M}}{\text{argmax}} \left( \min_{j \in \mathcal{P}} \tilde{\mathbf{D}}_{ij} + \epsilon \tilde{\mathbf{A}}_i \right)$
- 5:      $\mathcal{P}.\text{append}(x_{\text{new}})$ ,  $\mathcal{M}.\text{remove}(x_{\text{new}})$
- 6: **return**  $\mathcal{P}$

---

### 3.2 MULTI-SCALE SELF-ATTENTION

The self-attention mechanism in the Transformer is good at capturing global data patterns but ignores local context (Guo et al., 2020a). Exploiting local context has proven to be important for 3D spatial data such as 3D point clouds (Qi et al., 2017b). Therefore, we impose a distance-based constraint in self-attention in order to extract multi-scaled patterns from both local and global contexts.

Guo et al. (2020b) propose to use integer-based distance to limit attention to local word neighbors, which cannot be used in molecules. This is because different types of molecules have different densities and molecules of the same type have different spatial regularity, which results in the non-uniformity of interatomic distances. Normally, small molecules have a mean interatomic distance of 1-2 Å (Angstrom,  $10^{-10} m$ ), which is denser than large molecules like crystals and proteins with approximately 5 Å on average. To address that, we design a new multi-scale methodology to robustly capture details. Specifically, we mask atoms beyond a certain distance  $\tau_s$  (a real number as opposed to an integer in Guo et al. (2020b)) at each scale  $s$ . We denote  $d_{ij} = \|\mathbf{p}_i - \mathbf{p}_j\|_2$  as the Euclidean distance between the  $i$ -th and  $j$ -th atom. The attention calculation is modified as:

$$a_{ij}^{\tau_s} = \frac{\mathbf{q}_i \mathbf{k}_j^T \cdot \mathbf{1}_{\{d_{ij} < \tau_s\}}}{\sqrt{d_k}}, \mathbf{z}_i^{\tau_s} = \sum_{j=1}^N \sigma(a_{ij}^{\tau_s}) \mathbf{v}_j, \quad (5)$$

where  $\mathbf{1}_{\{d_{ij} < \tau_s\}}$  is the indicator function. For small molecules, Equation 5 can be complementally combined with Equation 4. Then features extracted from  $S$  different scales  $\{\tau_s\}_{s=1, \dots, S}$  as well as the informative global feature are concatenated together to form a multi-scale representation, denoted by  $\mathbf{z}'_i = \mathbf{z}_i^{\tau_1} \oplus \dots \oplus \mathbf{z}_i^{\tau_S} \oplus \mathbf{z}_i^{\text{global}} \in \mathbb{R}^{(S+1)d_k}$ . After that,  $\mathbf{z}'_i$  is forwarded into a multi-layer perceptron to be compressed as  $\mathbf{z}''_i$  with the original dimension  $d_k$ .

### 3.3 ATTENTIVE FARTHEST POINT SAMPLING

After having the atom embeddings  $\{\mathbf{z}''_i\}_{i=1, \dots, N}$ , we study how to obtain the molecular representation  $\mathbf{r}$ . For GNNs, several readout functions such as set2set (Vinyals et al., 2015) and GGNN (Gilmer et al., 2017) are invented. For Transformer architectures, one way is via a virtual atom. Though as Ying et al. (2021) state, it significantly improves the performance of existing models in the leaderboard of Open Graph Benchmark (Hu et al., 2020), this way concentrates more on close adjacent atoms and less on distant ones, and can lead to inadvertent over-smoothing of information propagation (Ishiguro et al., 2019). Besides, it is difficult to locate a virtual node in 3D space and build connections to existing atoms. The other way selects a subset of atoms via a downsampling algorithm named Farthest Point Search (FPS), but it ignores atomic differences and has sensitivity to outlier points (Pan et al., 2021) as well as uncontrollable randomness. To address these issues, we propose a new algorithm named AFPS. It aims to sample atoms by not merely spatial distances, but also their significance in terms of attention scores.

Specifically, we choose the virtual atom  $x_{\#}$  as the starting point and initialize two lists  $\mathcal{P} = \{x_{\#}\}$  and  $\mathcal{M} = \{1, \dots, N\}$  to store remaining candidate points. Then given an attention score matrix  $\mathbf{A} \in \mathbb{R}^{N \times N}$  and an interatomic distance matrix  $\mathbf{D} \in \mathbb{R}^{N \times N}$ ,  $\mathbf{A}$  are accumulated along columns<sup>2</sup> and  $\mathbf{D}$  is normalized between 0 and 1, resulting in  $\tilde{\mathbf{A}} \in \mathbb{R}^N$  and  $\tilde{\mathbf{D}}$ . We repeatedly move a point

<sup>2</sup>Each row of  $\mathbf{A}$  sums up to one after the *Softmax* operation.

$x_{new}$  from  $\mathcal{M}$  to  $\mathcal{P}$ , which ensures that  $x_{new}$  is as far from  $\mathcal{P}$  as possible by maximizing  $\tilde{D}_{ij}$  and also plays a crucial role in attention computation by maximizing  $\tilde{A}_i$ . Mathematically, the AFPS aims to the following objective

$$\sum_{i \in \mathcal{M}} \left( \min_{j \in \mathcal{P} \setminus \{i\}} \tilde{D}_{ij} + \epsilon \tilde{A}_i \right) \quad (6)$$

where  $\epsilon$  is a hyperparameter to balance those two different goals. This process is repeated until  $\mathcal{P}$  has reached  $K$  points. Algorithm 1 provides a greedy approximation solution to solve this AFPS optimization objective for sake of computational efficiency.

After that, sampled features  $\{\mathbf{z}_i''\}_{i \in \mathcal{P}}$  are gathered by a Global Average Pooling layer (Lin et al., 2013) to attain the molecular representation  $\mathbf{r} \in \mathbb{R}^{d_k}$ .

## 4 EXPERIMENT SETUP

We conduct comprehensive experiments with tasks and datasets from three domains: quantum chemistry, material science and proteomics. Table 1 summarises information of benchmark datasets, including the number of tasks and task types, the number of molecules and atom classes, the minimum and maximum number of atoms, the density (mean interatomic distances), and the mean structure complexity  $\bar{\phi}$  of all molecules in each dataset.

Table 1: Key statistics of datasets from three different domains.

| Category          | Dataset              | Tasks | Task Type  | Molecules | Atom Class | Min. Atoms | Max. Atoms | Density (Å) | $\bar{\phi}$ |
|-------------------|----------------------|-------|------------|-----------|------------|------------|------------|-------------|--------------|
| Quantum Chemistry | QM7                  | 1     | regression | 7,160     | 5          | 4          | 23         | 2.91        | 0.07         |
|                   | QM8                  | 12    | regression | 21,786    | 5          | 3          | 26         | 1.54        | 0.09         |
|                   | QM9                  | 12    | regression | 133,885   | 5          | 3          | 28         | 1.61        | 0.10         |
| Material Science  | CoRE-MOF             | 6     | regression | 10,068    | 77         | 10         | 10,560     | 5.73        | 0.54         |
| Protein           | PDBbind <sup>3</sup> | 1     | regression | 11,908    | 23         | 115        | 1,085      | 5.89        | 0.78         |

For QM9 and PDBbind dataset, we use the exact train/validation/test splits as Townshend et al. (2020). For others including CoRE-MOF, QM7, and QM8, 90% of the data is used for training and the rest is divided equally between validation and test like Chen et al. (2019c). More implementing details can be found in Appendix B.1

**Quantum Chemistry.** We test Molformer on the common QM7 (Blum & Reymond, 2009), QM8 (Ramakrishnan et al., 2015), and QM9 (Ramakrishnan et al., 2014) benchmark datasets. QM7 is a subset of GDB-13 and composed of 7K molecules with up to 7 heavy atom types. QM8 and QM9 are subsets of GDB-17 with 22k molecules and 133K molecule respectively.

We compare our approach with state-of-the-art baselines. TF\_Robust (Ramsundar et al., 2015) takes molecular fingerprints as the input. MPNN (Gilmer et al., 2017), Schnet (Schütt et al., 2018), and MEGNet (Chen et al., 2019c) as well as the variants of DMPNN (Yang et al., 2019) and MGCN (Lu et al., 2019), are all GCN-based models. AttentiveFP (Xiong et al., 2019) extends Graph Attention Networks (Veličković et al., 2017). Graph Transformer (Chen et al., 2019a) is built on longer-range dependencies in graph-structured data. DimeNet++ (Klicpera et al., 2020a) is a faster version of DimeNet (Klicpera et al., 2020b). SE(3)-Transformer (Fuchs et al., 2020) and LieTransformer (Hutchinson et al., 2021) are attention-based ENNs. SphereNet (Liu et al., 2021) utilizes a unified interface at different levels of granularity for 3D graphs. SpinConv (Shuaibi et al., 2021) models angular information between sets of neighboring atoms.

**Material Science.** We use the CoRE-MOF dataset (Chung et al., 2019) in this domain. Metal-organic frameworks (MOFs) are a kind of crystalline materials, widely used in storage, separation, catalysis, molecular censor, and drug release. CoRE-MOF contains over 14K MOFs with up to 77 element types. The particulars of this dataset are released in Appendix B.2.

We evaluate Molformer against two classic models for molecular and spatial information. PointNet++ (Qi et al., 2017b) is a hierarchical network that applies Pointnet (Qi et al., 2017a) recursively

<sup>3</sup>The total number of proteins in the full, unsplit PDBbind is 11K, but our experiment only uses 4K proteins at 30% sequence identity. Moreover, the number of atoms is the sum of both the pocket and molecules.

on the input 3D information. MPNN is a GCN model for molecular property prediction. Due to the large size of crystals (even much larger than proteins) and the limited machine memory, we cannot run other baselines such as Schnet even with a batch size of 1.

**Protein.** Forecasting the strength of the protein-molecule interaction remains a challenging but essential task for various applications such as drug discovery. We inspect Molformer’s ability of learning mutual relations between proteins and molecules on the PDBbind dataset (Wang et al., 2005). PDBbind provides detailed 3D coordinates of both ligands and proteins derived from experimental measurements. We follow Townshend et al. (2020) and split protein-ligand complexes by protein sequence identity at 30%. As for the target, we predict  $pS = -\log(S)$ , where  $S$  is the binding affinity in Molar unit. In addition, we only use the pocket of each protein and put pocket-ligand pairs together as the input.

We choose six baselines. DeepDTA (Öztürk et al., 2018) and DeepAffinity (Karimi et al., 2019) takes in pairs of ligand and protein SMILES as input. Cormorant (Anderson et al., 2019) is an ENN that represents each atom by its absolute 3D coordinates. Schnet, 3DCNN and 3DGCN (Townshend et al., 2020) are 3D molecular representation methods.

## 5 RESULTS AND DISCUSSION

We present and discuss experimental results in this section. Best performance is marked bold while the second best is underlined for clear comparison.

We visualize the distribution of  $\phi$  in different datasets<sup>4</sup>. From Figure 3, we observe that the mean of  $\phi$  of small molecules ( $\bar{\phi} < 0.15$ ) in the QM7, QM8 and QM9 datasets is much smaller compared with that of large molecules ( $\bar{\phi} > 0.5$ ) in the CoRE-MOF and the DPBbind datasets. It indicates that the small molecules have a less complex 3D structures than large molecules. Also, the overlap between the  $\phi$  distributions of small and large molecules are minor, which means the proposed metric  $\phi$  is a good indicator of small or large molecules.

### 5.1 PERFORMANCE COMPARISON WITH BASELINES

**Quantum Chemistry.** Table 2 and Table 3 document the overall results of Molformer and baselines on these three small molecule datasets. Like previous works, we compute the average Mean Absolute Error (MAE) of all 12 tasks on QM8. Molformer achieved the lowest MAE of 43.9 on QM7 and 0.009 on QM8, beating strong baselines like DMPNN and GROVE. While not all state-of-the-art on QM9, Molformer offers competitive performance in 5 property regression tasks. Particularly, we outperforms all Transformer-based ENNs, including SE(3)-Transformer and LieTransformer.

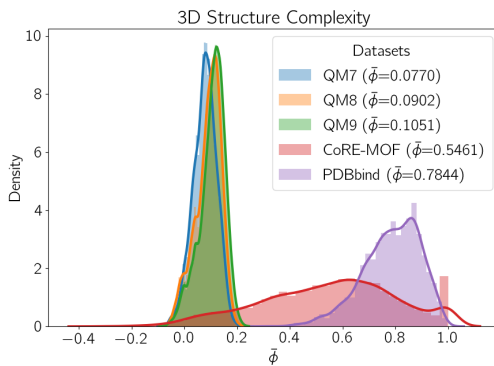


Figure 3: Structure complexity distributions of molecules in each dataset.

Table 2: Comparison of MAE on QM7 and QM8.

| Method                                     | QM7         | QM8          |
|--|-------------|--------------|
| TF-Robust (Ramsundar et al., 2015)         | 120.6       | 0.024        |
| MPNN (Gilmer et al., 2017)                 | 113.0       | 0.015        |
| Schnet (Schütt et al., 2018)               | 74.2        | 0.020        |
| DMPNN (Yang et al., 2019)                  | 105.8       | 0.014        |
| MGCN (Lu et al., 2019)                     | 77.6        | 0.022        |
| Attentive FP (Xiong et al., 2019)          | 126.7       | 0.028        |
| Graph Transformer (Chen et al., 2019a)     | 47.8        | 0.010        |
| GROVE <sub>base</sub> (Rong et al., 2020)  | 72.5        | 0.017        |
| GROVE <sub>large</sub> (Rong et al., 2020) | 72.6        | 0.012        |
| Molformer                                  | <b>43.9</b> | <b>0.009</b> |

<sup>4</sup>There we only calculate  $\phi$  of each single cell unit. But unlike small molecules and proteins, crystals have a periodic pattern. If we consider this periodic arrangement, the structure complexity of crystals is the highest.

Table 3: Comparison of MAE on QM9.

| Target (Unit)                                  | $\epsilon_{\text{HOMO}}$ (eV) | $\epsilon_{\text{LUMO}}$ (eV) | $\Delta\epsilon$ (eV) | $\mu$ (D)   | $\alpha$ (bohr $^3$ ) |
|--|-------------------------------|-------------------------------|-----------------------|-------------|-----------------------|
| MPNN (Gilmer et al., 2017)                     | .043                          | .037                          | .069                  | .030        | .092                  |
| Schnet (Schütt et al., 2018)                   | .041                          | .034                          | .063                  | .033        | .235                  |
| MEGNet full (Chen et al., 2019c)               | .038                          | .031                          | .061                  | .040        | .083                  |
| DimeNet++ (Klicpera et al., 2020a)             | .024                          | .019                          | .032                  | .029        | <b>.043</b>           |
| SE(3)-Transformer (Fuchs et al., 2020)         | .035                          | .033                          | .053                  | .051        | .142                  |
| LieTransformer-SE(3) (Hutchinson et al., 2021) | .033                          | .029                          | .052                  | .061        | .104                  |
| SphereNet (Liu et al., 2021)                   | <u>.024</u>                   | <b>.019</b>                   | <b>.032</b>           | <b>.026</b> | .047                  |
| SpinConv (Shuaibi et al., 2021)                | .026                          | .022                          | .047                  | .027        | .058                  |
| Molformer                                      | <b>.021</b>                   | .026                          | .039                  | .045        | .086                  |

**Material Science.** Table 4 shows quantitative results of Mean Square Error (MSE) on CoRE-MOF. Molformer largely outperforms two baselines, which proves its superiority of representing large molecules. Beyond that, we explore the periodic arrangement, a exclusive characteristic of crystals, for MOF’s property prediction. Experiments show that by expanding crystals, our model’s performance can be effectively enhanced with a big drop of MSE on all six targets. We owe these improvements to the ability of expansions to provide a more comprehensive view of crystal’s 3D conformations. We offer more discussions and experimental details in Appendix B.3.

Table 4: Comparison of MSE on CoRE-MOF.

| Target                        | LCD          | PLD          | D            | ASA          | NASA        | AV           |
|-------------------------------|--------------|--------------|--------------|--------------|-------------|--------------|
| PointNet++ (Qi et al., 2017b) | 3.138        | 2.755        | 0.119        | 592.1        | 47.3        | 0.055        |
| MPNN (Gilmer et al., 2017)    | 11.604       | 5.888        | 0.153        | 1227.2       | 51.7        | 0.134        |
| Molformer (w/o Expand)        | <u>1.819</u> | <u>1.550</u> | <u>0.020</u> | <u>265.8</u> | <u>31.0</u> | <u>0.020</u> |
| Molformer (w/ Expand)         | <b>1.608</b> | <b>1.396</b> | <b>0.014</b> | <b>185.8</b> | <b>28.4</b> | <b>0.019</b> |

**Protein.** Table 5 reports the Root-Mean-Squared Deviation (RMSD), the Pearson correlation ( $R_p$ ), and the Spearman correlation ( $R_s$ ) on PDBbind. Molformer achieves the lowest RMSD among all baselines and the best Pearson and Spearman correlations. As Wu et al. (2018) claim, appropriate featurizations which contains pertinent information is significant for PDBbind. However, an important observation is that deep learning approaches with the full exploitation of 3D geometric information can perform better than conventional methods like DeepDTA and DeepAffinity, which use a set of physicochemical descriptors but ignore 3D structure.

Table 5: Comparison of RMSD,  $R_p$ , and  $R_s$  on PDBbind.

| Method                             | Geometry | RMSD         | $R_p$        | $R_s$        |
|------------------------------------|----------|--------------|--------------|--------------|
| DeepDTA (Öztürk et al., 2018)      | Non-3D   | 1.565        | 0.573        | 0.574        |
| DeepAffinity (Karimi et al., 2019) | Non-3D   | 1.893        | 0.415        | 0.426        |
| Schnet (Schütt et al., 2018)       | 3D       | 1.892        | <u>0.601</u> | -            |
| Cormorant (Anderson et al., 2019)  | 3D       | <u>1.429</u> | 0.541        | 0.532        |
| 3DCNN (Townshend et al., 2020)     | 3D       | 1.520        | 0.558        | 0.556        |
| 3DGCN (Townshend et al., 2020)     | 3D       | 1.963        | 0.581        | <u>0.647</u> |
| Molformer                          | 3D       | <b>1.395</b> | <b>0.613</b> | <b>0.656</b> |

## 6 ABLATION STUDY AND DISCUSSION

**AFPS vs. FPS.** To have a vivid understanding of the atom sampling algorithm, we conducted a case study on a random crystal (see Figure 4). Points selected by FPS are randomized and exclude vital atoms like the heavy metal Nickel (Ni). With the adoption of AFPS, sampled points include Ni and Nitrogen (N) besides that they keep remote distances from each other. Moreover, FPS integrates too many features of trivial atoms like Hydrogen (H) while misses out key atoms, which will significantly smooth the molecular representations and lead to poor predictions. This illustrative example firmly shows the effectiveness of our AFPS to offset disadvantages of the conventional FPS in 3D molecular representation.

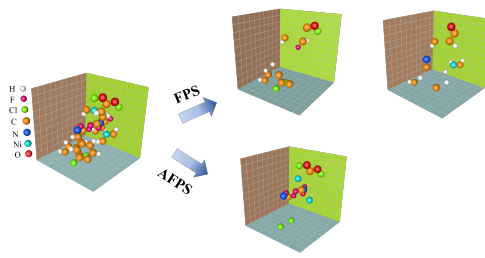


Figure 4: Sampled points using FPS and AFPS.

**CPE vs. APE.** As analyzed before, different types of molecules require different position encoding methods. Table 6 reveals that CPE excels in representing small molecules on QM7 and QM8. In those datasets, molecules have no more than 30 atoms and less complex structures, as indicated in Figure 3. The quantities computed in small molecule tasks relies more on relative positions instead of 3D conformations. On the other hand, in the circumstance of large molecules on CoRE-MOF and PDBbind, APE performs better than CPE. This is because properties of large molecules depend more upon their 3D conformations, which can be better described by absolute positions. In Appendix C.1, we provide more analytical results of each module.

Table 6: Comparison of different position encodings methods on large molecule datasets.

|     | PDBbind      |                |                | CoRE-MOF     |              |              |              |             |              |
|-----|--------------|----------------|----------------|--------------|--------------|--------------|--------------|-------------|--------------|
|     | RMSD         | R <sub>p</sub> | R <sub>s</sub> | LCD          | PLD          | D            | ASA          | NASA        | AV           |
| CPE | 1.474        | 0.545          | <b>0.534</b>   | 2.650        | 2.101        | 0.024        | <b>252.4</b> | 36.4        | 0.026        |
| APE | <b>1.386</b> | <b>0.575</b>   | 0.553          | <b>1.819</b> | <b>1.550</b> | <b>0.020</b> | 265.8        | <b>31.0</b> | <b>0.020</b> |

**Conformation Classification.** Molecules do not have a fixed 3D structure, but multiple conformations driven by rotatable bonds. Determining the multiple possible conformations of molecules is still an ongoing research topic (Hawkins, 2017). Few prior works analyze how multiple conformations affect 3D models. To fill this gap, we initialize a new task of conformation classification, where 3D models are required to classify molecules with diverse low-energy conformations. Figure 5 shows that Molformer performs perfectly on both GEOM-QM9 (Axelrod & Gomez-Bombarelli, 2020) and GEOM-CoRE-MOF datasets with approximately 100% accuracy. Experiments indicates that non-uniqueness of molecular conformations is not problematic for our model to take advantage of 3D structures. We leave more experimental details in Appendix C.2.

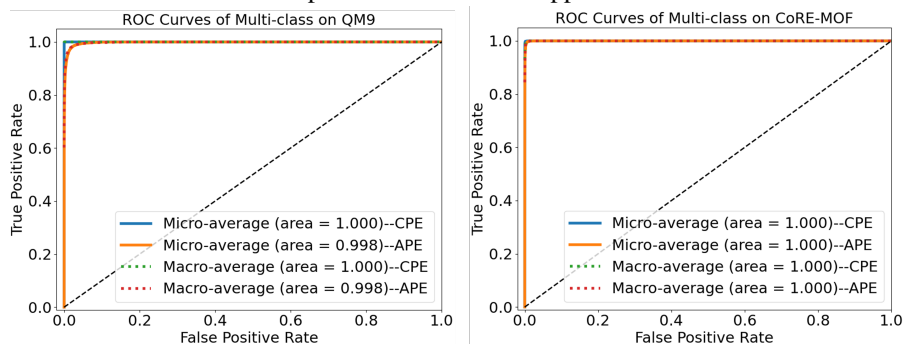


Figure 5: ROC curves of multi-class conformation classification.

## 7 RELATED WORKS

Deep learning has been widely applied to predict molecular properties during past decades. Small molecules are usually represented as lower-dimensional representations such as 1D linear sequence,

including amino acid sequences and SMILES (Weininger, 1988), or 2D chemical bond graphs. Graph-based models have been intensively tried (Schütt et al., 2017; Xie & Grossman, 2018).

In spite of that, more evidence indicates that 3D space structures lead to better modelling and superior performance. 3D models becomes a popular way to capture these complex geometries in a variety of bio-molecular applications using CNNs (Anand-Achim et al., 2021; Jiménez et al., 2018) and GNNs (Cho & Choi, 2018). Nonetheless, aforementioned methods have hardly been extended to the self-attention mechanism that is proven to be good at grabbing contextual feature (Tang et al., 2018) and long-range dependencies (Vaswani et al., 2017).

A few attempts have been undertaken to address that issue throughout Transformers. Initially, molecules are in the form of SMILES to obtain corresponding representations (Honda et al., 2019; Pesciullesi et al., 2020; Morris et al., 2020; Rao et al., 2021) and conduct pretraining (Chithrananda et al., 2020). Some researchers combine the characteristics of GNN and Transformer to solve generative tasks (Ingraham et al., 2019) or fulfill equivariance (Fuchs et al., 2020). To the best of our knowledge, we are the foremost to adapt a pure Transformer model with well designed modules for learning representations of 3D molecule.

## 8 CONCLUSION

In this study, we present a universal neural architecture designed for 3D molecular representations. Our Molformer augments the self-attention mechanism with multiplicative scales to catch local features from neighboring atoms. In order to make a full use of spatial information, ATPE takes different position encoding strategies for various molecules. Furthermore, a simple but efficient down-sampling algorithm called AFPS is introduced to better group representations of an entire molecule. Our experiments show the superiority of our model on various scientific domains.

## REFERENCES

Clarivate Analytics. Web of science, 2017.

Namrata Anand-Achim, Raphael Ryuichi Eguchi, Irimpan I Mathews, Carla P Perez, Alexander Derry, Russ B Altman, and Possu Huang. Protein sequence design with a learned potential. *bioRxiv*, pp. 2020–01, 2021.

Brandon Anderson, Truong-Son Hy, and Risi Kondor. Cormorant: Covariant molecular neural networks. *arXiv preprint arXiv:1906.04015*, 2019.

Kenneth Atz, Francesca Grisoni, and Gisbert Schneider. Geometric deep learning on molecular representations. *arXiv preprint arXiv:2107.12375*, 2021.

Simon Axelrod and Rafael Gomez-Bombarelli. Geom: Energy-annotated molecular conformations for property prediction and molecular generation. *arXiv preprint arXiv:2006.05531*, 2020.

Minkyung Baek, Frank DiMaio, Ivan Anishchenko, Justas Dauparas, Sergey Ovchinnikov, Gyu Rie Lee, Jue Wang, Qian Cong, Lisa N. Kinch, R. Dustin Schaeffer, Claudia Millán, Hahnbeom Park, Carson Adams, Caleb R. Glassman, Andy DeGiovanni, Jose H. Pereira, Andria V. Rodrigues, Alberdina A. van Dijk, Ana C. Ebrecht, Diederik J. Opperman, Theo Sagmeister, Christoph Buhlheller, Tea Pavkov-Keller, Manoj K. Rathinaswamy, Udit Dalwadi, Calvin K. Yip, John E. Burke, K. Christopher Garcia, Nick V. Grishin, Paul D. Adams, Randy J. Read, and David Baker. Accurate prediction of protein structures and interactions using a three-track neural network. *Science*, 2021. ISSN 0036-8075. doi: 10.1126/science.abj8754.

Lorenz C Blum and Jean-Louis Reymond. 970 million druglike small molecules for virtual screening in the chemical universe database gdb-13. *Journal of the American Chemical Society*, 131(25): 8732–8733, 2009.

Yuchao Chai, Xue Han, Weiyao Li, Shanshan Liu, Sikai Yao, Chong Wang, Wei Shi, Ivan da Silva, Pascal Manuel, Yongqiang Cheng, et al. Control of zeolite pore interior for chemoselective alkyne/olefin separations. *Science*, 368(6494):1002–1006, 2020.

Benson Chen, Regina Barzilay, and Tommi Jaakkola. Path-augmented graph transformer network. *arXiv preprint arXiv:1905.12712*, 2019a.

Chao Chen, Guanbin Li, Ruijia Xu, Tianshui Chen, Meng Wang, and Liang Lin. Clusternet: Deep hierarchical cluster network with rigorously rotation-invariant representation for point cloud analysis. In *Proceedings of the IEEE/CVF Conference on Computer Vision and Pattern Recognition*, pp. 4994–5002, 2019b.

Chi Chen, Weike Ye, Yunxing Zuo, Chen Zheng, and Shyue Ping Ong. Graph networks as a universal machine learning framework for molecules and crystals. *Chemistry of Materials*, 31(9):3564–3572, 2019c.

Seyone Chithrananda, Gabriel Grand, and Bharath Ramsundar. Chemberta: Large-scale self-supervised pretraining for molecular property prediction. *arXiv preprint arXiv:2010.09885*, 2020.

Hyeoncheol Cho and Insung S Choi. Three-dimensionally embedded graph convolutional network (3dgcn) for molecule interpretation. *arXiv preprint arXiv:1811.09794*, 2018.

Yongchul G Chung, Emmanuel Haldoupis, Benjamin J Bucior, Maciej Haranczyk, Seulchan Lee, Hongda Zhang, Konstantinos D Vogiatzis, Marija Milisavljevic, Sanliang Ling, Jeffrey S Camp, et al. Advances, updates, and analytics for the computation-ready, experimental metal–organic framework database: Core mof 2019. *Journal of Chemical & Engineering Data*, 64(12):5985–5998, 2019.

Georgy Derevyanko, Sergei Grudinin, Yoshua Bengio, and Guillaume Lamoureux. Deep convolutional networks for quality assessment of protein folds. *Bioinformatics*, 34(23):4046–4053, 2018.

Philipp Dufter, Martin Schmitt, and Hinrich Schütze. Position information in transformers: An overview. *arXiv preprint arXiv:2102.11090*, 2021.

Fabian B Fuchs, Daniel E Worrall, Volker Fischer, and Max Welling. Se (3)-transformers: 3d roto-translation equivariant attention networks. *arXiv preprint arXiv:2006.10503*, 2020.

Justin Gilmer, Samuel S Schoenholz, Patrick F Riley, Oriol Vinyals, and George E Dahl. Neural message passing for quantum chemistry. In *International conference on machine learning*, pp. 1263–1272. PMLR, 2017.

Colin R Groom, Ian J Bruno, Matthew P Lightfoot, and Suzanna C Ward. The cambridge structural database. *Acta Crystallographica Section B: Structural Science, Crystal Engineering and Materials*, 72(2):171–179, 2016.

Meng-Hao Guo, Jun-Xiong Cai, Zheng-Ning Liu, Tai-Jiang Mu, Ralph R Martin, and Shi-Min Hu. Pct: Point cloud transformer. *arXiv preprint arXiv:2012.09688*, 2020a.

Qipeng Guo, Xipeng Qiu, Pengfei Liu, Xiangyang Xue, and Zheng Zhang. Multi-scale self-attention for text classification. In *Proceedings of the AAAI Conference on Artificial Intelligence*, volume 34, pp. 7847–7854, 2020b.

Paul CD Hawkins. Conformation generation: the state of the art. *Journal of Chemical Information and Modeling*, 57(8):1747–1756, 2017.

Adrián Hernández and José M Amigó. Attention mechanisms and their applications to complex systems. *Entropy*, 23(3):283, 2021.

Shion Honda, Shoi Shi, and Hiroki R Ueda. Smiles transformer: Pre-trained molecular fingerprint for low data drug discovery. *arXiv preprint arXiv:1911.04738*, 2019.

Weihua Hu, Matthias Fey, Marinka Zitnik, Yuxiao Dong, Hongyu Ren, Bowen Liu, Michele Catasta, and Jure Leskovec. Open graph benchmark: Datasets for machine learning on graphs. *arXiv preprint arXiv:2005.00687*, 2020.

Michael J Hutchinson, Charline Le Lan, Sheheryar Zaidi, Emilien Dupont, Yee Whye Teh, and Hyunjik Kim. Lietransformer: Equivariant self-attention for lie groups. In *International Conference on Machine Learning*, pp. 4533–4543. PMLR, 2021.

John Ingraham, Vikas K Garg, Regina Barzilay, and Tommi Jaakkola. Generative models for graph-based protein design. 2019.

Katsuhiko Ishiguro, Shin-ichi Maeda, and Masanori Koyama. Graph warp module: an auxiliary module for boosting the power of graph neural networks in molecular graph analysis. *arXiv preprint arXiv:1902.01020*, 2019.

José Jiménez, Miha Skalic, Gerard Martinez-Rosell, and Gianni De Fabritiis. K deep: protein–ligand absolute binding affinity prediction via 3d-convolutional neural networks. *Journal of chemical information and modeling*, 58(2):287–296, 2018.

Chaitanya Joshi. Transformers are graph neural networks. *The Gradient*, 2020.

John Jumper, Richard Evans, Alexander Pritzel, Tim Green, Michael Figurnov, Olaf Ronneberger, Kathryn Tunyasuvunakool, Russ Bates, Augustin Žídek, Anna Potapenko, Alex Bridgland, Clemens Meyer, Simon A A Kohl, Andrew J Ballard, Andrew Cowie, Bernardino Romera-Paredes, Stanislav Nikolov, Rishabh Jain, Jonas Adler, Trevor Back, Stig Petersen, David Reiman, Ellen Clancy, Michal Zielinski, Martin Steinegger, Michalina Pacholska, Tamas Berghammer, Sebastian Bodenstein, David Silver, Oriol Vinyals, Andrew W Senior, Koray Kavukcuoglu, Pushmeet Kohli, and Demis Hassabis. Highly accurate protein structure prediction with AlphaFold. *Nature*, 2021. doi: 10.1038/s41586-021-03819-2. (Accelerated article preview).

Mostafa Karimi, Di Wu, Zhangyang Wang, and Yang Shen. Deepaffinity: interpretable deep learning of compound–protein affinity through unified recurrent and convolutional neural networks. *Bioinformatics*, 35(18):3329–3338, 2019.

Sungwon Kim, Juhwan Noh, Geun Ho Gu, Alan Aspuru-Guzik, and Yousung Jung. Generative adversarial networks for crystal structure prediction. *ACS central science*, 6(8):1412–1420, 2020.

Diederik P Kingma and Jimmy Ba. Adam: A method for stochastic optimization. *arXiv preprint arXiv:1412.6980*, 2014.

Johannes Klicpera, Shankari Giri, Johannes T Margraf, and Stephan Günnemann. Fast and uncertainty-aware directional message passing for non-equilibrium molecules. *arXiv preprint arXiv:2011.14115*, 2020a.

Johannes Klicpera, Janek Groß, and Stephan Günnemann. Directional message passing for molecular graphs. *arXiv preprint arXiv:2003.03123*, 2020b.

Hailiang Li, YC Adele, Yang Liu, Du Tang, Zhibin Lei, and Wenye Li. An augmented transformer architecture for natural language generation tasks. In *2019 International Conference on Data Mining Workshops (ICDMW)*, pp. 1–7. IEEE, 2019.

Min Lin, Qiang Chen, and Shuicheng Yan. Network in network. *arXiv preprint arXiv:1312.4400*, 2013.

Xuanqing Liu, Hsiang-Fu Yu, Inderjit Dhillon, and Cho-Jui Hsieh. Learning to encode position for transformer with continuous dynamical model. In *International Conference on Machine Learning*, pp. 6327–6335. PMLR, 2020.

Yi Liu, Limei Wang, Meng Liu, Xuan Zhang, Bora Oztekin, and Shuiwang Ji. Spherical message passing for 3d graph networks. *arXiv preprint arXiv:2102.05013*, 2021.

Chengqiang Lu, Qi Liu, Chao Wang, Zhenya Huang, Peize Lin, and Lixin He. Molecular property prediction: A multilevel quantum interactions modeling perspective. In *Proceedings of the AAAI Conference on Artificial Intelligence*, volume 33, pp. 1052–1060, 2019.

Paul Morris, Rachel St. Clair, William Edward Hahn, and Elan Barenholtz. Predicting binding from screening assays with transformer network embeddings. *Journal of Chemical Information and Modeling*, 60(9):4191–4199, 2020.

Lien Ai Nguyen, Hua He, and Chuong Pham-Huy. Chiral drugs: an overview. *International journal of biomedical science: IJBS*, 2(2):85, 2006.

Hakime Öztürk, Arzucan Özgür, and Elif Ozkirimli. Deepdta: deep drug–target binding affinity prediction. *Bioinformatics*, 34(17):i821–i829, 2018.

Guillaume Pagès, Benoit Charmettant, and Sergei Grudinin. Protein model quality assessment using 3d oriented convolutional neural networks. *Bioinformatics*, 35(18):3313–3319, 2019.

Xuran Pan, Zhuofan Xia, Shiji Song, Li Erran Li, and Gao Huang. 3d object detection with point-former. In *Proceedings of the IEEE/CVF Conference on Computer Vision and Pattern Recognition*, pp. 7463–7472, 2021.

Adam Paszke, Sam Gross, Francisco Massa, Adam Lerer, James Bradbury, Gregory Chanan, Trevor Killeen, Zeming Lin, Natalia Gimelshein, Luca Antiga, et al. Pytorch: An imperative style, high-performance deep learning library. *Advances in neural information processing systems*, 32: 8026–8037, 2019.

Giorgio Pesciullesi, Philippe Schwaller, Teodoro Laino, and Jean-Louis Reymond. Transfer learning enables the molecular transformer to predict regio-and stereoselective reactions on carbohydrates. *Nature communications*, 11(1):1–8, 2020.

Niklas Pfriem, Peter H Hintermeier, Sebastian Eckstein, Sungmin Kim, Qiang Liu, Hui Shi, Lara Milakovic, Yuanshuai Liu, Gary L Haller, Eszter Baráth, et al. Role of the ionic environment in enhancing the activity of reacting molecules in zeolite pores. *Science*, 372(6545):952–957, 2021.

Charles R Qi, Hao Su, Kaichun Mo, and Leonidas J Guibas. Pointnet: Deep learning on point sets for 3d classification and segmentation. In *Proceedings of the IEEE conference on computer vision and pattern recognition*, pp. 652–660, 2017a.

Charles R Qi, Li Yi, Hao Su, and Leonidas J Guibas. Pointnet++: Deep hierarchical feature learning on point sets in a metric space. *arXiv preprint arXiv:1706.02413*, 2017b.

Raghunathan Ramakrishnan, Pavlo O Dral, Matthias Rupp, and O Anatole von Lilienfeld. Quantum chemistry structures and properties of 134 kilo molecules. *Scientific Data*, 1, 2014.

Raghunathan Ramakrishnan, Mia Hartmann, Enrico Tapavicza, and O Anatole Von Lilienfeld. Electronic spectra from tddft and machine learning in chemical space. *The Journal of chemical physics*, 143(8):084111, 2015.

Bharath Ramsundar, Steven Kearnes, Patrick Riley, Dale Webster, David Konerding, and Vijay Pande. Massively multitask networks for drug discovery. *arXiv preprint arXiv:1502.02072*, 2015.

Roshan Rao, Nicholas Bhattacharya, Neil Thomas, Yan Duan, Xi Chen, John Canny, Pieter Abbeel, and Yun S Song. Evaluating protein transfer learning with tape. *Advances in neural information processing systems*, 32:9689, 2019.

Roshan Rao, Jason Liu, Robert Verkuij, Joshua Meier, John F Canny, Pieter Abbeel, Tom Sercu, and Alexander Rives. Msa transformer. *bioRxiv*, 2021.

Yu Rong, Yatao Bian, Tingyang Xu, Weiyang Xie, Ying Wei, Wenbing Huang, and Junzhou Huang. Self-supervised graph transformer on large-scale molecular data. *arXiv preprint arXiv:2007.02835*, 2020.

Kristof T Schütt, Farhad Arbabzadah, Stefan Chmiela, Klaus R Müller, and Alexandre Tkatchenko. Quantum-chemical insights from deep tensor neural networks. *Nature communications*, 8(1):1–8, 2017.

Kristof T Schütt, Huziel E Sauceda, P-J Kindermans, Alexandre Tkatchenko, and K-R Müller. Schnet—a deep learning architecture for molecules and materials. *The Journal of Chemical Physics*, 148(24):241722, 2018.

Andrew W Senior, Richard Evans, John Jumper, James Kirkpatrick, Laurent Sifre, Tim Green, Chongli Qin, Augustin Žídek, Alexander WR Nelson, Alex Bridgland, et al. Improved protein structure prediction using potentials from deep learning. *Nature*, 577(7792):706–710, 2020.

Muhammed Shuaibi, Adeesh Kolluru, Abhishek Das, Aditya Grover, Anuroop Sriram, Zachary Ulissi, and C Lawrence Zitnick. Rotation invariant graph neural networks using spin convolutions. *arXiv preprint arXiv:2106.09575*, 2021.

Gongbo Tang, Mathias Müller, Annette Rios, and Rico Sennrich. Why self-attention? a targeted evaluation of neural machine translation architectures. *arXiv preprint arXiv:1808.08946*, 2018.

Nathaniel Thomas, Tess Smidt, Steven Kearnes, Lusann Yang, Li Li, Kai Kohlhoff, and Patrick Riley. Tensor field networks: Rotation-and translation-equivariant neural networks for 3d point clouds. *arXiv preprint arXiv:1802.08219*, 2018.

Raphael Townshend, Rishi Bedi, Patricia Suriana, and Ron Dror. End-to-end learning on 3d protein structure for interface prediction. *Advances in Neural Information Processing Systems*, 32:15642–15651, 2019.

Raphael JL Townshend, Martin Vögele, Patricia Suriana, Alexander Derry, Alexander Powers, Yianni Laloudakis, Sidhika Balachandar, Brandon Anderson, Stephan Eismann, Risi Kondor, et al. Atom3d: Tasks on molecules in three dimensions. *arXiv preprint arXiv:2012.04035*, 2020.

Ashish Vaswani, Noam Shazeer, Niki Parmar, Jakob Uszkoreit, Llion Jones, Aidan N Gomez, Łukasz Kaiser, and Illia Polosukhin. Attention is all you need. In *Advances in neural information processing systems*, pp. 5998–6008, 2017.

Petar Veličković, Guillem Cucurull, Arantxa Casanova, Adriana Romero, Pietro Lio, and Yoshua Bengio. Graph attention networks. *arXiv preprint arXiv:1710.10903*, 2017.

Oriol Vinyals, Samy Bengio, and Manjunath Kudlur. Order matters: Sequence to sequence for sets. *arXiv preprint arXiv:1511.06391*, 2015.

Benyou Wang, Lifeng Shang, Christina Lioma, Xin Jiang, Hao Yang, Qun Liu, and Jakob Grue Simonsen. On position embeddings in bert. In *International Conference on Learning Representations*, 2020.

Renxiao Wang, Xueliang Fang, Yipin Lu, Chao-Yie Yang, and Shaomeng Wang. The pdbsbind database: methodologies and updates. *Journal of medicinal chemistry*, 48(12):4111–4119, 2005.

Xiaolong Wang, Ross Girshick, Abhinav Gupta, and Kaiming He. Non-local neural networks. In *Proceedings of the IEEE conference on computer vision and pattern recognition*, pp. 7794–7803, 2018.

Yuyang Wang, Jianren Wang, Zhonglin Cao, and Amir Barati Farimani. Molclr: Molecular contrastive learning of representations via graph neural networks. *arXiv preprint arXiv:2102.10056*, 2021.

David Weininger. Smiles, a chemical language and information system. 1. introduction to methodology and encoding rules. *Journal of chemical information and computer sciences*, 28(1):31–36, 1988.

Yulun Wu, Nicholas Choma, Andrew Chen, Mikaela Cashman, Érica T Prates, Manesh Shah, Verónica G Melesse Vergara, Austin Clyde, Thomas S Brettin, Wibe A de Jong, et al. Spatial graph attention and curiosity-driven policy for antiviral drug discovery. *arXiv preprint arXiv:2106.02190*, 2021.

Zhenqin Wu, Bharath Ramsundar, Evan N Feinberg, Joseph Gomes, Caleb Geniesse, Aneesh S Pappu, Karl Leswing, and Vijay Pande. Moleculenet: a benchmark for molecular machine learning. *Chemical science*, 9(2):513–530, 2018.

Tian Xie and Jeffrey C Grossman. Crystal graph convolutional neural networks for an accurate and interpretable prediction of material properties. *Physical review letters*, 120(14):145301, 2018.

Zhaoping Xiong, Dingyan Wang, Xiaohong Liu, Feisheng Zhong, Xiaozhe Wan, Xutong Li, Zhaojun Li, Xiaomin Luo, Kaixian Chen, Hualiang Jiang, et al. Pushing the boundaries of molecular representation for drug discovery with the graph attention mechanism. *Journal of medicinal chemistry*, 63(16):8749–8760, 2019.

Hang Yan, Bocao Deng, Xiaonan Li, and Xipeng Qiu. Tener: adapting transformer encoder for named entity recognition. *arXiv preprint arXiv:1911.04474*, 2019.

Kevin Yang, Kyle Swanson, Wengong Jin, Connor Coley, Philipp Eiden, Hua Gao, Angel Guzman-Perez, Timothy Hopper, Brian Kelley, Miriam Mathea, et al. Analyzing learned molecular representations for property prediction. *Journal of chemical information and modeling*, 59(8):3370–3388, 2019.

Chengxuan Ying, Tianle Cai, Shengjie Luo, Shuxin Zheng, Guolin Ke, Di He, Yanming Shen, and Tie-Yan Liu. Do transformers really perform bad for graph representation? *arXiv preprint arXiv:2106.05234*, 2021.

Yuning You, Tianlong Chen, Yongduo Sui, Ting Chen, Zhangyang Wang, and Yang Shen. Graph contrastive learning with augmentations. *Advances in Neural Information Processing Systems*, 33:5812–5823, 2020.

Haitao Zhang, Gye Won Han, Alexander Batyuk, Andrii Ishchenko, Kate L White, Nilkanth Patel, Anastasiia Sadybekov, Beata Zamlynny, Michael T Rudd, Kaspar Hollenstein, et al. Structural basis for selectivity and diversity in angiotensin ii receptors. *Nature*, 544(7650):327–332, 2017.

Shuo Zhang, Yang Liu, and Lei Xie. Molecular mechanics-driven graph neural network with multiplex graph for molecular structures. *arXiv preprint arXiv:2011.07457*, 2020.

Alex Zhavoronkov, Yan A Ivanenkov, Alex Aliper, Mark S Veselov, Vladimir A Aladinskiy, Anastasiya V Aladinskaya, Victor A Terentiev, Daniil A Polykovskiy, Maksim D Kuznetsov, Arip Asadulaev, et al. Deep learning enables rapid identification of potent ddr1 kinase inhibitors. *Nature biotechnology*, 37(9):1038–1040, 2019.

## A ADAPTIVE POSITION ENCODING

### A.1 3D MOLECULAR STRUCTURE COMPLEXITY

Few efforts have been paid to measure the molecular structure complexity in the 3D space. There we define a simple but efficient way to evaluate it. First, we need to find the smallest cuboid to contain the molecule with a length, height, width of  $l, h, w$ . We denote  $a = \min(l, h, w)$ ,  $c = \max(l, h, w)$  and  $b$  is the second largest of  $l, h, w$ .

A naive metric  $\phi$  can be defined as  $\phi = \frac{a}{b} + \frac{b}{c} - 1$  with a range of  $[-1, 1]$ . If  $\phi$  is close to 1, then the molecular structure complexity is high. While the structure complexity is low if  $\phi$  is far from 1. However, the above metric takes no account of the molecular density. For instance, we compare a small molecule with  $a = 1, b = 10, c = 10$  to a large molecule with  $a = 10, b = 100, c = 100$ . Though they share the same  $\phi$ , the large molecule usually has a far more complex internal 3D structure than the small molecule due to the fact that the large molecule contains richer atoms than the smaller one. To overcome this problem, we design the Equation 2. Under this measurement, the small molecule with is clearly distinguished from the large molecule by the factor  $\tanh(\frac{N}{100})$ .

### A.2 IMPLEMENTATION OF ABSOLUTE POSITION ENCODING

We choose the sinusoidal functions to encode absolute positions for large molecules. Specifically, we map coordinates  $\mathbf{p}_i$  of each axis into the feature dimension  $d_{model}$  as  $(\mathbf{E}_{p_i^x}, \mathbf{E}_{p_i^y}, \mathbf{E}_{p_i^z})$  by sinusoidal functions (Vaswani et al., 2017) concurrently. Taking the  $x$ -axis for example,  $\mathbf{E}_{(p_i^x, 2j)} = \sin(\frac{\lambda p_i^x}{10000^{2j}/d_{model}})$ ,  $\mathbf{E}_{(p_i^x, 2j+1)} = \cos(\frac{\lambda p_i^x}{10000^{2j}/d_{model}})$ , where a hyperparameter  $\lambda$  is multiplied to avoid the great variance per position across dimensions (Li et al., 2019). Those embeddings are merged with atom embeddings  $\mathbf{E}'_i = \mathbf{x}_i + \mathbf{E}_{p_i^x} + \mathbf{E}_{p_i^y} + \mathbf{E}_{p_i^z}$ .

Learnable position embedding (Liu et al., 2020) cannot be applied there, since 3D coordinates are all decimal numbers and it is hard to discrete them. In comparison to learnable position embeddings, sinusoidal patterns keep positional values fixed and requires no additional trainable parameters (Wang et al., 2020). Besides, they are capable of handling decimal coordinates as well as unseen coordinates (Liu et al., 2020). It is also translation invariant (Wang et al., 2020) and can indicate the relative distance to some extent because of  $\mathbf{E}_{p_i^x + \Delta p^x}^T \mathbf{E}_{p_i^x} \perp\!\!\!\perp \Delta p^x$  (Yan et al., 2019).

### A.3 ENCODING CHIRAL MOLECULES WITH ABSOLUTE POSITIONS

Molecular properties are roto-translation invariant (Atz et al., 2021). However, some molecules are chiral and their chiral properties are dependent to the absolute configuration of their stereogenic centers, and thus non-invariant to reflection, as we claim in Proposition 1. For example, drug isomers exhibit markedly different pharmacological and toxicological properties (Nguyen et al., 2006).

**Proposition 1** *Let  $\mathbf{T}$  describe any rotations and translations in  $\mathbb{R}^3$ . For any chiral molecule  $\mathbf{S}_1 = (\mathbf{X}_1, \mathbf{P}_1)$  with a Euclidean distance matrix  $\mathbf{D}_1$ , there exists another molecule  $\mathbf{S}_2 = (\mathbf{X}_2, \mathbf{P}_2)$  with  $\mathbf{X}_2 = \mathbf{X}_1$  and  $\mathbf{D}_2 = \mathbf{D}_1$  such that  $\mathbf{P}_2 \neq \mathbf{T} \circ \mathbf{P}_1$  for any transformation  $\mathbf{T}$ .*

Recent popular molecular learning methods such as ENNs and GNNs are unable to differentiate isomers. This is because ENNs comprise only roto-translation equivariance and GNNs are built on atomic connections. Graphs of chiral molecules and their counterparts are equivalent, and therefore identical for GNNs. Moreover, we claim that encoding molecules using relative positions is also not a feasible solution. As shown in Figure 6, for some special molecules such as bromochlorofluoromethane, its stereocenter can never be obtained through any rotations or translations even though they share the same interatomic distance matrix.

Relative distances are not able to distinguish chiral molecules. Two molecules with the same interatomic distance matrix can have mirroring 3D structures (see Figure 6), resulting in different properties. In contrast, using absolute positions directly represent differences between patterns in 3D space, and thus is more suitable to maintain the spatial information.

We analyse absolute position encoding is a proper way to distinguish chiral molecules. Unfortunately, few previous works paid attention to this task, and we are not able to find available datasets for the time being. We leave out the examination of our theoretical analysis for future work.

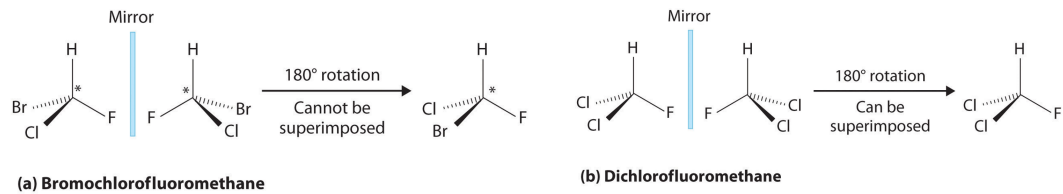


Figure 6: Examples of chiral and achiral molecules. (a) Bromochlorofluoromethane is a chiral molecule whose stereocenter is designated with an asterisk. Rotation of its mirror image does not generate the original structure. To superimpose the mirror images, bonds must be broken and reformed. (b) In contrast, dichlorofluoromethane and its mirror image can be rotated.

## B EXPERIMENTAL SETUP

### B.1 EXPERIMENTAL DETAILS

**Molformer Architecture.** Our Molformer has 6 multi-scale self-attention layers, and each layer has 3 scales and 8 heads. Normally, scales are set as  $[\frac{\rho}{2}, \rho, 2\rho]$ , where  $\rho$  is the density of a corresponding dataset. The number of selected atoms  $K$  in the AFPS is set as 4 and 10 for small and large molecule datasets, respectively.  $\lambda$  in APE is kept as 10. We use ReLU as the activation function and a dropout rate of 0.1 for all layers. The input embedding size is 512 and the hidden size for FFN is 2048.

**Training Details.** We use Pytorch (Paszke et al., 2019) to implement Molformer and data parallelism in two GeForce RTX 3090. An Adam (Kingma & Ba, 2014) optimizer is used and a lambda scheduler is enforced to adjust it. We apply no weight decay there. Each model is trained with 300 epochs, except for PDBbind where we solely train the model for 30 epochs. For QM7 and QM8, we use a batch size of 64 and a learning rate of  $10^{-4}$ . For QM9, we use a batch size of 256 and a learning rate of  $10^{-3}$ . For PDBbind, we choose a batch size of 16 and a learning rate of  $10^{-4}$ . For CoRE-MOF, we choose a batch size of 8 and a learning rate of  $5 * 10^{-5}$ . All hyper-parameters are tuned based on validation sets. For small molecules and PDBbind, we impose no limitation on the length of molecules, while for CoRE-MOF, we truncate the length of crystals with a maximum length of 1024. No additional atom features are included other than the atom type. For all datasets but PDBbind, we normalise the values of each regression task by mean and the standard deviation of the training set. We used grid search to tune the hyper-parameters of our model and baselines based on the validation dataset.

### B.2 CORE-MOF DESCRIPTIONS

CoRE-MOF is obtained from the Cambridge Structural Database (Groom et al., 2016) and a Web of Science (Analytics, 2017) search. It is derived through semi-automated reconstruction of disordered structures using a topology-based crystal generator. It contains MOFs’ 3D coordinates, adsorption performances, and pore analytics. Table 7 explains the specific names of chemical properties that are used as targets in our experiment.

Table 7: The targets used in our experiment of material science.

| Abbreviation | Term                        | Dataset Unit       | Our Unit           |
|--------------|-----------------------------|--------------------|--------------------|
| LCD          | Largest Cavity Diameter     | Å                  | Å                  |
| PLD          | Pore Limiting Diameter      | Å                  | Å                  |
| D            | Density                     | cm <sup>3</sup> /g | cm <sup>3</sup> /g |
| ASA          | Accessible Surface Area     | m <sup>2</sup> /g  | m <sup>2</sup> /kg |
| NASA         | Non-accessible Surface Area | m <sup>2</sup> /g  | m <sup>2</sup> /kg |
| AV           | Accessible Volume           | cm <sup>3</sup> /g | cm <sup>3</sup> /g |

### B.3 EXPANSION OF CRYSTALS

**Setup.** Unlike small molecules and proteins, crystals are periodic arranged and their cell units are not unique owing to different possible cutting perspectives. Though each cell unit contains the same number and same types of atoms, their geometric information can be totally different. For instance, two atoms in one cell unit are close to each other but might be far away in another. This leads to a problem that models might distinguish two cells units of the same crystal into two different molecules. We try to alleviate this trouble by expanding the cell units.

We adopt the methodology of Kim et al. (2020) to extend the cell unit in CoRE-MOF. Providing 3D structure of a crystal ( $p^x, p^y, p^z$ ) and its lattice parameters ( $x_c, y_c, z_c, \alpha, \beta, \gamma$ ), where  $x_c, y_c, z_c$  are coordinates of the three axes and  $\alpha, \beta, \gamma$  are angles, 3D coordinates of the new cell unit can be obtained by Equation 7, where  $n, m, k$  are any integers. When  $n = m = k = 0$ , that is exactly the original cell unit. We walk  $n, m, k$  through the value space of  $-1, 0, 1$  and attain new crystals with  $3 \times 3 \times 3 = 27$  cell units.

$$\begin{aligned} p_{n,m,k}^x &= p^x + x_c + nx_c + my_c \cos \gamma + kz_c \cos \beta \\ p_{n,m,k}^y &= p^y + y_c + my_c \sin \gamma + kz_c \frac{\cos \alpha - \cos \beta \cos \gamma}{\sin \gamma} \\ p_{n,m,k}^z &= p^z + z_c + kz_c \sqrt{\sin^2 \beta - \frac{(\cos \alpha - \cos \beta \cos \gamma)^2}{\sin^2 \gamma}} \end{aligned} \quad (7)$$

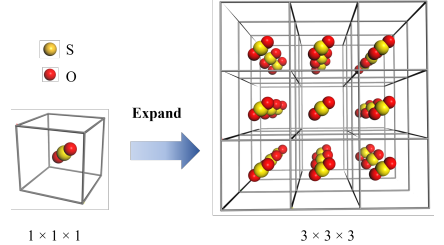


Figure 7: Example of expanding a single cell unit into a  $3 \times 3 \times 3$  one.

**Results.** We checkout the effect of this extension. Results (see Table 4) prove that our model’s performance is considerably improved by expanding the cell unit. In addition, this expansion can be regarded as a way of data augmentation similar to the atom mask technique in molecular representation learning (You et al., 2020; Wang et al., 2021), and self-supervised learning such as contrastive learning can be applied in those augmented crystals.

## C ADDITIONAL EXPERIMENTAL RESULTS

### C.1 EFFECTS OF EACH COMPONENT

We investigate the effectiveness of different modules of our Molformers. Table 8 shows some results on QM7 and QM8 datasets. As we can see, MSA and CPE substantially boost model’s performance. AFPS produces slight improvements on these small molecular datasets, but reduces RMSD significantly from 1.412 to 1.386 on PDBbind. AFPS is better suited to large molecules than small molecules, because there is little difference to sample a large portion of atoms from small molecules compared with aggregating all of them.

Table 8: Effects of each module on QM7 and QM8.

|   | MSA | AFPS | CPE | QM7         | QM8           |
|---|-----|------|-----|-------------|---------------|
| 1 | -   | -    | -   | 63.2        | 0.0186        |
| 2 | -   | -    | ✓   | 50.1        | 0.0104        |
| 3 | -   | ✓    | ✓   | 48.7        | 0.0103        |
| 4 | ✓   | -    | ✓   | <b>43.9</b> | <b>0.0098</b> |
| 5 | ✓   | ✓    | ✓   | <u>45.8</u> | <u>0.0099</u> |

## C.2 CONFORMATION CLASSIFICATION

**Task and Data.** In order to explore the influence of multiple conformations, we introduce a new task, conformation classification, to evaluate model’s capacity to differentiate molecules with various low-energy conformations. We use the recent GEOM-QM9 (Axelrod & Gomez-Bombarelli, 2020) and construct a GEOM-CoRE-MOF from CoRE-MOF for experiments.

More specifically, GEOM-QM9 is an extension to QM9 dataset. It contains multiple conformations for most molecules, while the original QM9 only contains one. As for GEOM-Core-MOF, we utilize the translation invariance of crystals’ cell units to form the dataset. Figure 8 illustrates that a same crystal can have many cell units with completely different 3D coordinates if the coordinates system varies. The calculation process are as follows, where we use the same notations in Appendix B.3 to depict a crystal’s 3D structure.

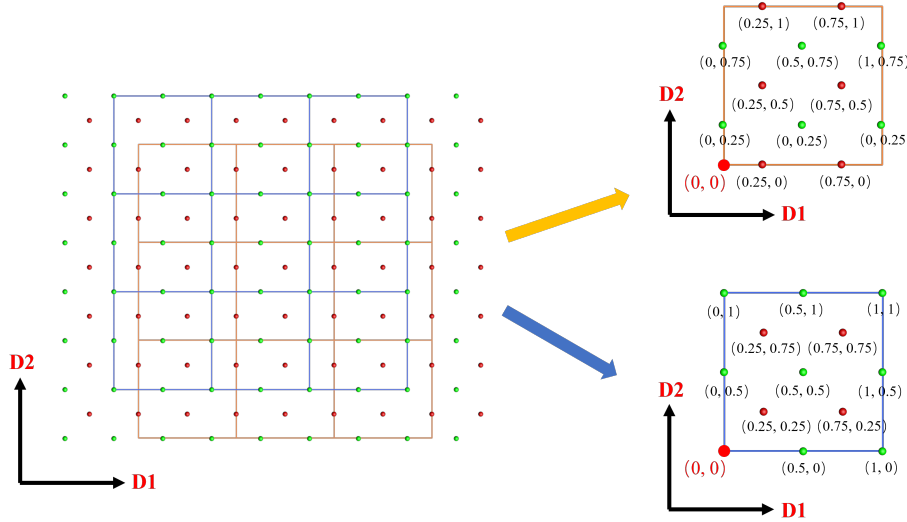


Figure 8: Coordinates of a same crystal under two different coordinate systems. We vision them in a 2D perspective for simplicity and explicitness.

First, the crystal is translated with a given distance vector  $(\Delta p^x, \Delta p^y, \Delta p^z)$ . Then an intermediate variable  $m$  is computed as  $m = \lfloor \frac{p^z + \Delta p^z}{z_c \sqrt{\sin^2 \beta - \frac{(\cos \alpha - \cos \beta \cos \gamma)^2}{\sin^2 \gamma}}} \rfloor$  to update the coordinates:

$$\begin{aligned} p_{(1)}^x &= p^x + \Delta p^x - mz_c \cos \beta \\ p_{(1)}^y &= p^y + \Delta p^y - mz_c \frac{\cos \alpha - \cos \beta \cos \gamma}{\sin \gamma} \\ p_{new}^z &= p^z + \Delta p^z - mz_c \sqrt{\sin^2 \beta - \frac{(\cos \alpha - \cos \beta \cos \gamma)^2}{\sin^2 \gamma}} \end{aligned} \quad (8)$$

After that, another variable  $n$  is calculated as  $n = \lfloor \frac{p_{(1)}^z}{z_c \sqrt{\sin^2 \beta - \frac{(\cos \alpha - \cos \beta \cos \gamma)^2}{\sin^2 \gamma}}} \rfloor$  to update the coordinates:

$$\begin{aligned} p_{new}^y &= p_{(1)}^y - y_c \sin \gamma \lfloor \frac{p_{(1)}^y - nz_c \frac{\cos \alpha - \cos \beta \cos \gamma}{\sin \gamma}}{y_c \sin \gamma} \rfloor \\ p_{(2)}^x &= p_{(1)}^x - y_c \cos \gamma \lfloor \frac{p_{(1)}^x - nz_c \frac{\cos \alpha - \cos \beta \cos \gamma}{\sin \gamma}}{y_c \sin \gamma} \rfloor \end{aligned} \quad (9)$$

The last step is to update only the coordinate of  $x$ -axis as blow, and we get the final translated coordinates  $(p_{new}^x, p_{new}^y, p_{new}^z)$  of that crystal.

$$p_{new}^x = p_{(2)}^x - x_c \left\lfloor \frac{p_{(2)}^x - nz_c \cos \beta}{x_c} \right\rfloor \quad (10)$$

We randomly pick several crystals and use techniques from Kim et al. (2020) to calculate their different 3D structures. We randomly draw 1000 different molecules from GEOM-QM9 and GEOM-CoRE-MOF, respectively, each with 20 different conformations. Models are required to distinguish the molecular type given different conformations. We take a half of each molecular conformations as the training set and another half as the test split. Since it is a multi-class classification problem with 1000 classes, we compute the micro-average and macro-average ROC-AUC as well as the accuracy for numerical evaluations.

**Results.** Figure 5 and Table 9 show that our model achieves superior performance on all three metrics and has a strong robustness to the non-uniqueness of molecular conformations. We report accuracy (Acc.), micro-average ROC-AUC (Micro.), and macro-average ROC-AUC (Macro.) for evaluations.

Table 9: Performance of Molformer in the conformation classification task.

|     | GEOM-QM9 |        |        | GEOM-CoRE-MOF |        |        |
|-----|----------|--------|--------|---------------|--------|--------|
|     | Acc.     | Micro. | Macro. | Acc.          | Micro. | Macro. |
| CPE | 0.999    | 1.000  | 1.000  | 0.953         | 1.000  | 1.000  |
| APE | 0.840    | 0.998  | 0.998  | 0.931         | 1.000  | 1.000  |